Membrane performance with plug screw feeder pressate: operating conditions and membrane properties

Dal-Cin, M. M.; Striez, Carolyn; Tweddle, T. A.; McLellan, F.; Ramamurthy, P.

Publisher's version / Version de l'éditeur:

Desalination, 105, 1996

ELSEVIER

Desalination 105 (1996) 229–244

DESALINATION

Membrane performance with plug screw feeder pressate: operating conditions and membrane properties*

M.M. Dal-Cin[a**], C.N. Striez[a], T.A. Tweddle[a], F. McLellan[b], P. Ramamurthy[c]

[a]*Institute for Chemical Process and Environmental Technology, National Research Council of Canada, Ottawa, Canada*
Fax (613) 941-2529
[b]*Abitibi-Price, Sheridan Park Technology Center, Mississauga, Ontario, Canada*
[c]*PAPRICAN, Pointe Claire, Quebec, Canada*

Received 21 September 1995; accepted 3 December 1995

Abstract

Membrane performance can be significantly affected by operating conditions. The effects of transmembrane pressure and cross flow velocity are discussed for various membranes during ultrafiltration of a pulp mill effluent. The effluent contained suspended solids, colloidal particles such as resin and fatty acids and materials with a wide molecular weight distribution. This effluent had severe membrane fouling characteristics, the nature of which complicated interpretation of the results. A variety of commercially available membranes made with different polymers and pore sizes were evaluated. Permeation experiments were performed using thin-channel, flat sheet, test cells. Cross-flow velocities varied from 0.4 to 1.2 m/s and the transmembrane pressure from 345 to 1,035 kPa. Flux decline occurred by several mechanisms and the selection of the membrane material, pore size and the operating conditions determined the relative contribution of these mechanisms. A modified series resistance model using flux loss ratios qualitatively explained changes in membrane performance under different operating conditions.

Keywords: Ultrafiltration; Fouling; Series resistance model; Pulp mill

1. Introduction

Membrane operations is one of several competing technologies which can be used in the pulp and paper industry to meet increasingly stringent requirements for effluent treatment. Pressure-driven membrane processes, including reverse osmosis (RO), nano-, ultra- and microfiltration, are of interest in such applications. These are primarily distinguished by the increasing pore size or molecular weight cut-off (MWCO). The acceptance of membrane technology has been hampered by fouling which results in a decline of the permeate flux with

*Issued as NRCC No. 37603.

**Corresponding author.

PII S0011-9164(96)00080-X

operating time. This results in larger membrane surface area requirements and shorter membrane life leading to higher capital and operating costs.

Membrane flux decline observed during permeation is the cumulative effect of several mechanisms. These include adsorption, steric hindrance, permeate viscosity, pore plugging, concentration polarization and gel layer formation. Flux decline due to adsorption can result in pure water flux reductions of 80–90% [1]. Steric hinderance occurs when solutes of sizes comparable to the pore sizes retard the flow of solvent through the pores [2,3]. If the viscosity of the permeate is higher than that of water, fluxes will be lower than the pure water permeability even in the absence of fouling. Pore plugging can occur by adsorption or physical entrapment of a solute in the pore. The degree of pore plugging is determined by the relative size of the solute and pore as well as the operating conditions [4]. Concentration polarization describes the accumulation of solutes at the surface of a membrane due to the preferential transport of solvent through the membrane. The higher solute concentration at the surface increases the osmotic pressure, thereby reducing the effective driving force. In an extreme case, the concentration at the membrane surface may reach levels at which the solute precipitates, forms a gel or exhibits non-Newtonian behavior [5]. Gel formation may occur over a longer time frame compared to osmotic effects [6] and is highly dependent on the feed and module hydrodynamics. In these cases the deposit or gel can determine the retention characteristics and represents an additional hydraulic resistance to permeate flow.

Minimization of membrane fouling has obvious benefits; the means to achieve this goal depend on the dominant fouling mechanisms. The descriptions above suggest when fouling can be expected and point to possible solutions. Adsorption can be controlled by understanding and manipulating the membrane-solute interactions. This can be accomplished by selecting an appropriate membrane material or by altering the properties of the feed, for example, the pH or salinity can be changed or flocculants added to the feed. Pore plugging is best controlled by preventing the solute from entering the membrane matrix. This requires selecting a membrane with a MWCO much smaller than the solute(s). The pore size distribution of the membrane and size distribution of the feed, if any, should not overlap or at least be minimized. Concentration polarization and gel layer formation are determined by the hydrodynamics of the membrane module, flux, solute concentration and molecular weight. Efficient mass transfer at the membrane surface minimizes driving force losses due to osmotic pressure effects and minimizes the thickness of the gel or deposited layer. Mass transfer at the membrane surface can be improved by increasing the shear rate with higher cross flow velocities, using turbulence promoters [7] or unsteady flow [8–10].

In this work we have evaluated membrane performance with plug screw feeder pressate, PSFP, under different operating conditions by varying the mass transfer or cross-flow velocity (CFV) at the membrane surface and the transmembrane pressure (TMP). Changes in membrane performance observed by varying these conditions are related to the membrane material and pore size by the contributions of the fouling mechanisms. These are measured using a modified series resistance model based on flux loss ratios.

2. Theory

2.1. Flux models

The pure water permeation rate through a new membrane can be described by:

$$J_0 = \frac{\Delta P}{\mu (R_m)} \tag{1}$$

where ΔP is the transmembrane pressure drop, μ is the permeate viscosity and R_m is the resistance due to the membrane alone.

Flux losses during ultrafiltration occur through various mechanisms, which can be modelled

phenomenologically using a series resistance model. The model has been used in various forms, consisting of a single hydraulic resistance due to the polarized layer to a more general form attributing individual resistances to different fouling mechanisms [11,12]:

$$J_v = \frac{\Delta P}{\mu\left(R_m + R_a + R_{pp} + R_{cp}\right)} \tag{2}$$

where J_v is the product rate, R_a, R_{pp} and R_{cp} are the resistances to flow due to adsorptive fouling, pore plugging and concentration polarization or gel layer formation, respectively.

Assuming the permeate viscosity to be the same and taking the ratio of J_0 and J_v gives

$$\frac{J_0}{J_v} = \frac{R_t}{R_m} = \frac{R_m + R_f}{R_m} = 1 + \frac{R_f}{R_m} \tag{3}$$

where R_f is the resistance due to all possible fouling mechanisms (R_a+R_{pp}+R_{cp}). The individual resistance components can be determined from the pure water permeabilities for membranes at various stages of testing.

The R_a term is determined using the pure water flux after contacting the membrane with the feed material, J_a, in the absence of a transmembrane pressure for 3 h. Adsorptive fouling may be more severe under permeation conditions with the PSFP. This would be a result of the higher concentrations at the membrane surface due to polarization. Permeation may also expose surfaces deep in the membrane structure to the effluent which were not accessible in the absence of a transmembrane pressure. However, this would have most likely compromised the estimate for R_{pp}, particularly for more open (high MWCO) membranes. Concentrating the feed material to simulate polarization conditions was not possible without altering its composition (i.e., evaporation would have removed volatile components, RO could have removed trace components etc.).

The R_{pp} term can be determined from the pure water flux after rinsing the membrane without washing, J_f, using the previously calculated R_a term. R_{cp} can be calculated in a similar manner using J_v. Resistances calculated in this manner are often expressed as a percentage of the overall resistance, R_t. The resistances in Eq. (2) have been shown (under review) to be dependent on the numerical sequence of their evaluation. Typically, the effect of adsorptive fouling is underestimated and that due to concentration polarization is overestimated. The flux loss ratios, D_i, for each fouling mechanism are determined as a fraction of the overall fouling resistance and more accurately describe the importance of each fouling mechanism to flux decline. They are expressed as a percentages, including a term for the membrane itself:

$$D_a = \frac{R_f}{R_t} \times \frac{J_0 - J_a}{J_0 - J_f} \times 100 \tag{4}$$

$$D_{pp} = \frac{R_f}{R_t} \times \frac{J_a - J_f}{J_0 - J_v} \times 100 \tag{5}$$

$$D_{cp} = \frac{R_f}{R_t} \times \frac{J_f - J_v}{J_0 - J_v} \times 100 \tag{6}$$

$$D_m = \frac{R_m}{R_t} \times 100 \tag{7}$$

2.2. Operating variables: effect on flux

Operating variables can include parameters such as transmembrane pressure, cross-flow velocity, temperature and pH. This work concentrated on the effects of the transmembrane pressure and cross flow velocity. The effects of pH or additives (such as flocculants or lime) were not studied as they may present problems in other unit operations at the pulp mill or generate a new waste stream. The operating temperature will have a significant effect on flux via the diffusivity of solutes and fluid

viscosity on the retentate side. The most pronounced effect will be on the permeate viscosity as predicted by the Hagen-Poiseuille flow.

With pure water or solvents, the flux will be proportional to the TMP as described by Eq. (2). The effect of the transmembrane pressure on the flux with solutions can be described by a mass balance of the film theory at the membrane surface [13]:

$$J_v = \frac{D}{\delta} \ln\left(\frac{C_m - C_p}{C_b - C_p}\right) = k \ln\left(\frac{C_m - C_p}{C_b - C_p}\right) \quad (8)$$

where C_m, C_b, and C_p are the solute concentrations at the membrane surface, bulk and permeate respectively. D, δ and k are the solute diffusivity, thickness of the polarized layer and mass transfer co-efficient. In actual practice the flux increase is often much less than expected for a given pressure increase and in some cases the flux may remain constant. As the product rate increases, C_m also increases, resulting in a higher osmotic pressure. Eventually, increases in the osmotic pressure negate any further gain in the product rate and the limiting flux is attained. In the case of gel/cake formation, a limiting flux is also attained in which the gel/cake layer thickness and/or density increase at higher pressures.

Increasing the mass transfer coefficient either by changing the cross-flow velocity or module design results in a higher flux. Gekas and Hallström [14] reviewed existing correlations for the Sherwood number and applied them to membrane operations. The Sherwood number is related to the mass transfer co-efficient which is in turn related to the Reynolds and Schmidt numbers,

$$Sh = \frac{kd_h}{D} = (\text{constant})\, Re^{\,a} Sc^{\,b} \quad (9)$$

where d_h is the hydraulic diameter. The Reynolds and Schmidt numbers are given by

$$Re = \frac{d_h u_0 \rho}{\mu} \quad \text{and} \quad Sc = \frac{\mu}{\rho D} \quad (10)$$

where u_0 and ρ are the feed velocity and density, respectively. The exponent of Re varied from 0.5 to 1 depending on the conditions and range of Re under consideration, but was generally close to 0.75 for turbulent flow and 0.33 for laminar flow.

The film theory has been criticized for being overly simplistic. The porosity and roughness of the membrane and changing physical properties are not accounted for. Gekas and Hallström proposed a friction factor, f, to account for the membrane surface roughness. The changing physical properties, viscosity and diffusivity, were accounted for by a correction factor $(Sc/Sc_m)^{0.11}$, using properties of the solution at the membrane surface and in the bulk fluid. Aimar and Field [15] criticized this correction factor because it is based on heat transfer analogues for heating. In such a situation the fluid viscosity at the wall is lower than the bulk, which is the opposite of that encountered during concentration polarization. They suggest an alternative correction factor which can be estimated by

$$k = k_0 \left(\frac{\mu_b}{\mu_m}\right)^{0.27} \quad (11)$$

According to Eq. (11), the effective mass transfer at the membrane surface will always be less than that predicted by Sherwood number correlations.

Lahoussine-Turcaud et al. [16] and others have described the deposition of particles by comparing their transport velocities towards the membrane surface to their back transport by Brownian diffusion (υ_B), lateral migration (υ_L) or shear induced diffusion (υ_S). The transport velocity to the surface is approximated by the permeate flux while the back transport velocities can be estimated from

$$\upsilon_B = \frac{k_B T}{3\pi\mu r d_p} \quad (12)$$

$$\upsilon_L = \frac{\rho u_0^2 d_p^3}{32\mu r^2} \quad (13)$$

$$\upsilon_S = \frac{0.05 u_0 d_p^2}{4r^2} \quad (14)$$

where k_B is the Boltzman constant, r is the radius of a hollow fiber or the center line distance between parallel plates, u_0 is the center line maximum velocity and d_p is the particle diameter. The particle velocities are approximated in Fig. 1 for the test cells used in this work and using the properties of water at 25°C. A typical low ultrafiltration flux observed in this work was 25 LMH, corresponding to 6.94×10^{-6} m/s. The lateral migration velocity determines which particles will deposit on the membrane surface for fluxes >25 LMH. Using Eq. (13), this corresponds to particle diameters <2.6 microns. Larger particles will deposit at higher fluxes.

2.3. Operating variables: effect on retention

When the intrinsic retention, $f = 1-C_p/C_m$, is assumed to be constant, then Eq. (8) can be rewritten to show the effect of the product rate and mass transfer coefficient on the observed retention, F:

$$F = \frac{f}{f+(1-f)\exp\left(\frac{J_v}{k}\right)} \quad (15)$$

The observed retention will decrease if the product rate is increased and k is constant. The observed retention will also decrease when the mass transfer coefficient decreases. In both situations the solute concentration at the membrane surface increases, resulting in lower observed retentions as C_p increases and C_b remains constant.

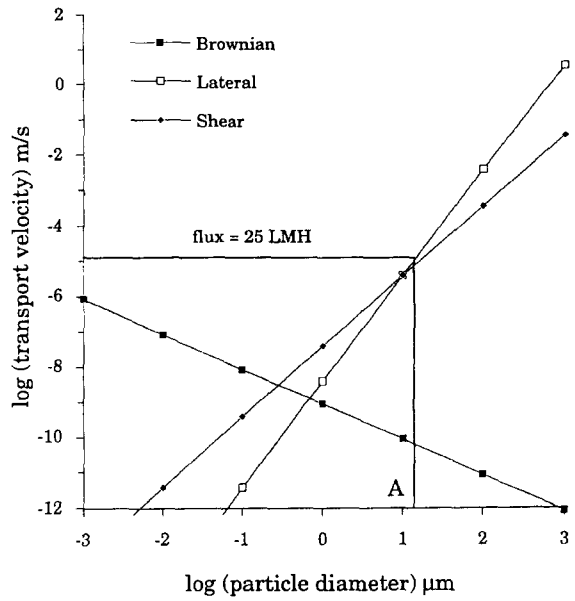

Fig. 1. Back transport velocities for lateral migration, Brownian and shear induced diffusion. Particles smaller than A will deposit on the membrane surface for a flux of 25 LMH.

The effect of the transmembrane pressure or mass transfer on retention with gel layer formation is difficult to predict. If the gel layer determines the retention characteristics, the effect of pressure may be negligible or cause F to increase. The effect of higher mass transfer rates may also be difficult to predict. If the gel is stable or thick, then the retention would not be expected to change significantly. When the gel layer is unstable or very thin, increasing the mass transfer may disrupt the gel layer. In this situation the retention may change and will be determined by the membrane properties.

3. Materials

The feed material used in this work was the PSFP from the chip digester of a semi-chemical mechanical pulping mill. Samples of PSFP were taken during regular operation of the pulp mill

Table 1
Composition of PSFP, 100-mesh filtrate

pH	5.7
Electrical conductivity, μΩ	5,100
Dissolved solids, mg/l	12,600
Suspended solids, mg/l	1,700
Total organic carbon, mg/l	5,670
Biological oxygen demand, mg/l	5,250
Resin and fatty acids, mg/l	432
Lignin sol, mg/l	2,400
Lignin insol, mg/l	1,900
Volatile[a] acids, mg/l	920
Sugars, m/l	2,680

[a]Primarily acetic acid.

and refrigerated at 2°C until tested. The feed was used as received except for prescreening with a 400 mesh sieve to remove large fibers. A summary of the constituents is given in Table 1. Fig. 2 shows the multi-modal molecular weight distribution of PSFP components ranging from ~4.0×10^6 to <100 Da. The high molecular weight material represents cellulosics and lignins. The lower molecular weight material ~200–400 is most likely sugars and possibly any non-colloidal resin and fatty acids (RFAs) while simple organic acids are represented by the lower molecular weight peaks. GPC analysis was performed using a Perkin Elmer Series 3B pump, Waters Model 410 RI detector and Waters Ultrahydragel 500, 250 and 125 columns. De-ionized water was used as the solvent at 1 ml/min and 40°C. Samples were pre-filtered with single use Minisart NML, 0.45 μm, microfilters from Sartorius.

Particle size distributions were determined for PSFP after screening with a 400-mesh sieve. Non-screened PSFP contains much larger particles including wood fibers up to 1–10 mm in diameter. The particle size distribution of PSFP is shown in Fig. 3 and was determined with a Granulometer HR 850 (Cilas-Alcatel). The particle sizes covered a broad range from 0.1 μm to 20–60 μm depending on the size analysis range used. The upper limit was set by the pre-screening which is equivalent to 37 μm. The median particle size varied between 1–11μm with the variation

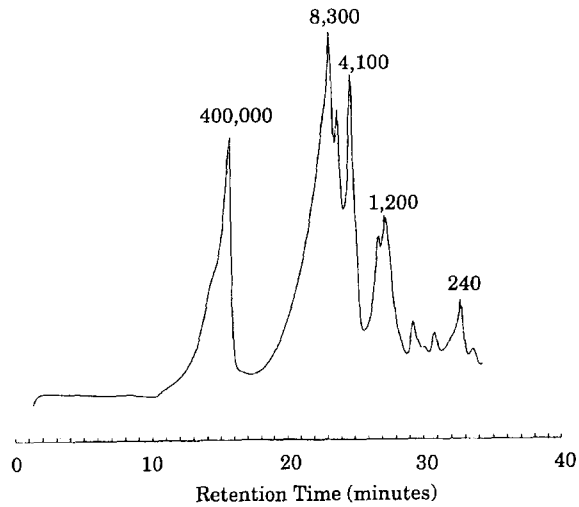

Fig. 2. Molecular weight distribution of PSFP as determined by GPC. Molecular weight is shown for selected peaks.

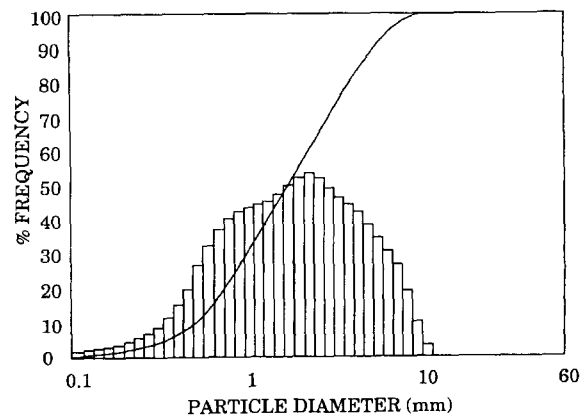

Fig. 3. Typical particle size distribution of PSFP as determined by dynamic light scattering with a Granoulemeter HR 850. PSFP pre-screened with 400-mesh sieve.

being the result of slight changes in the shape of the distribution or changing the analysis range. Particle size analysis (not shown) was also performed using a Malvern Zetasizer 3 for the range 5 nm to 5 μm. No material was observed below 0.1–0.5 μm on repeated measurements.

The exact composition and particle size distribution of the PSFP changes constantly and

depends on many variables. Some of these are the current operating characteristics of the digester, seasonal variations, source of wood chips and storage time of the chips before use. PSFP also undergoes undetermined physical/chemical changes if not refrigerated. These changes occur in less than 24 h at 50°C and are visually characterized by a darkening of the samples from a light brown to a darker shade. The odor also changes from that of freshly cut wood to a pungent/acrid character. Feed samples of PSFP in the UF test system were replaced before these changes occurred.

RFAs form colloidal suspensions in water and may be associated with other materials in the PSFP. The molecular weight of RFAs is typically ~300 g/mol. Analysis of feed and permeate samples showed that ultrafiltration with >100,000 MWCO membranes removed ~70–90% of the RFAs. This suggests that the RFAs exist as micelles and/or are bound to larger cellulosics, lignins or polysaccharides in the effluent. The larger components may have a fixed amount of water ad/absorbed in their structure. This mixture could form a gel on the membrane surface during ultrafiltration [17]. Woerner and McCarthy [18] described the ultrafiltration flux of Kraft black liquor as being dominated by a gel layer. While KBL and PSFP are quite different, lignins represent a major component of both liquids and were shown to form gels in experiments using model solutions [19].

The membranes used to study the effects of operating variables were a subset of those used in another study with the same PSFP and are summarized in Table 2. The membranes were selected to represent extreme cases of high/low adsorptive fouling, small and large pore sizes to highlight pore plugging, etc. They represent a broad range of materials and pore sizes. Materials included PVDF, polysulfone, polyamide-imide, regenerated cellulose and several thin-film composites (TFC). MWCOs ranged from nano-filtration (92% NaCl retention) to the upper limit of ultrafiltration (>500 K MWCO).

Table 2
Flux loss ratios due to adsorption, pore plugging and concentration polarization/gel layer formation for various membranes with PSFP. D terms evaluated at 0.8 m/s and 345 kPa

Membrane	Manufacturer	Rated MWCO	Material	% D_m	% D_a	% D_{pp}	% D_{cp}
LSY PVD1	Hydranautics	92% NaCl	TFC[b]	61	48	− 8	− 1
DESAL 5	Desalination	200	TFC	89	−45	66	−10
PLAC	Millipore	1,000	RC[c]	49	11	0	39
T66	NRCC	8,000	PAI[d]	34	27	17	22
C-10	Hoescht-Celanese	10,000	RC	43	4	−13	66
G50	Desalination Systems	15,000	TFC	45	−51	61	44
T64	NRCC	20,000	PAI	2	88	6	4
C-30	Hoescht-Celanese	30,000	RC	25	−13	6	82
HFM180	Koch	18,000[a]	PVDF[e]	8	− 9	81	20
GR40	DDS	100,000	PS[f]	N/A			
GR10	DDS	500,000	PS	N/A			

[a]Recently re-rated to 100,000 MWCO by Koch.
[b]Thin-film composite. [c] Regenerated cellulose.
[d]Polyamide-imide. [e] Polyvinylidenefluoride.
[f]Polysulfone.

4. Procedures

The thin-channel test cells used make use of an impinging feed to promote mixing at the membrane surface (Fig. 4). The feed enters the test cell perpendicular to the center of the circular membrane coupon and then flows radially to the perimeter where it is collected and goes to the next cell. The effective surface area was 14.5×10^{-4} m^2 with a channel thickness, H, of 5.08×10^{4} m at the periphery. The channel height is machined such that a uniform velocity profile is maintained across the radius of the cell. The cross flow velocities used were 0.4, 0.8 and 1.2 m/s corresponding to Reynolds numbers of ~ 400, 800 and 1,200, respectively, with water at 25°C. The impinging flow pattern and short flow path promote mixing beyond that expected for the estimated Reynolds numbers. Twelve test cells were used simultaneously in a configuration of four parallel banks with three test cells in series. The pressure drop across a bank of cells was <14 kPa at 0.8 m/s.

Permeate from the test cells was recycled to the feed tank at all times except during flux measurements, which were determined gravimetrically. Permeate collected for flux measurements was returned to the feed tank. Negligible volumes were required for retention analysis. The observed retention, F, was based on total organic carbon (TOC, Shimadzu 5000) reduction using

$$F = \frac{TOC_{\text{feed}} - TOC_{\text{permeate}}}{TOC_{\text{feed}}} \tag{16}$$

Permeate samples were generally clear solutions and analysed without further processing. Suspended solids were removed from the feed samples using a single use filter (Minisart NML, 0.2 μm, Sartorius) and then diluted to the appropriate concentration for TOC analysis. This sample treatment may result in TOC values for the feed being underestimated. As this procedure was used for all samples, performance comparisons based on retention were valid. Retentions can be given a global tolerance of ±5% even though the accuracy of the TOC is considerably better at ±1%. The largest source of error was associated with the feed sample prefiltering and dilution. TOC was used to evaluate the retention because the method has proved reliable in the past, is very fast and economical. The large number of analyses performed in the overall study precluded analysis for individual components or classes of components such as resin and fatty acids, biological oxygen demand (BOD) or chemical oxygen demand (COD).

The operating temperature was fixed at 50°C to simulate the expected operating temperature of a full-scale membrane system. Higher temperatures would increase fluxes, but supplemental heating would be required and may not be economical. Higher temperatures would approach the operating limit of the cellulosic membranes.

The experimental procedure adopted was a compromise between achieving true steady-state performance, avoiding complications due to aging feed and expected hysterisis due to pressure effects. Membranes were operated at 345 kPa and 0.8 m/s for one day with 10 l of PSFP until fluxes had stabilized. A stabilization stage was required to minimize confounding the effect of

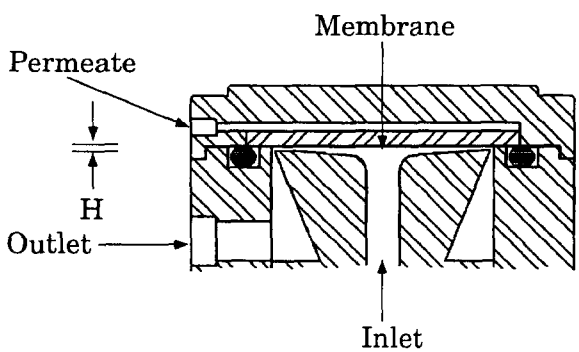

Fig. 4. Cross-flow rest cell configuration. Effective permeation area is 14.5×10^{-4} m^2. The channel height, H, at the outer perimeter is 5.08×10^{-4}.

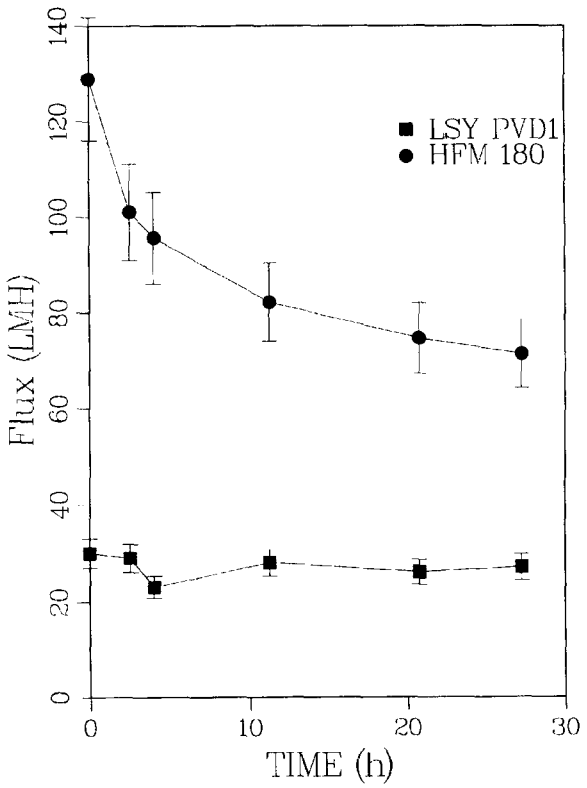

The feed was replaced with a new 10 l sample of PSFP after the initial 24 h period and fluxes allowed to stabilize again. The feed sample was changed to avoid confusing the effects of changing operating conditions with those of aging feed. A new 10 l sample of PSFP was added before each pressure increase (690 and 1,035 kPa) and fluxes were allowed to stabilize before changing the operating conditions. All the PSFP came from a single 200 l batch. As will be seen in the Results and Discussion, the stabilization times were not sufficient and complicated interpretation of the results.

The effects of pressure and cross-flow velocity were studied using a three-level factorial design at all combinations of pressure and cross-flow velocity. Pressures were 345, 690 and 1,035 kPa and cross-flow velocities were 0.4, 0.8 and 1.2 m/s. The relationship between flux and pressure may display some hysterisis due to pore plugging effects. This hysterisis would be more pronounced with large pore membranes and higher transmembrane pressures. As such, replicates at the center point or the standard operating conditions (0.8 m/s and 345 kPa) would

Table 3
Fluxes of various membranes with PSFP at different operating conditions. Data are sorted based on the TMP and increasing cross-flow velocity at a given TMP

Membrane	Flux (LMH)										Flux 10 / Flux 1 (%)
LSY PVD1	25	27	26	28	48	54	34	45	51	20	74
DESAL 5	24	25	23	36	58	56	44	56	82	24	94
PLAC	33	33	31	35	56	57	37	50	47	19	58
T66	44	45	41	43	57	77	44	60	83	36	81
C-10	85	82	83	58	117	142	53	111	76	35	43
G50	59	58	55	45	64	93	48	73	71	47	81
T64	24	28	27	34	43	44	35	45	43	18	65
C-30	90	119	115	73	143	160	65	133	87	43	36
HFM180	83	91	94	47	81	101	43	69	67	30	33
GR40	84	101	98	50	87	99	43	70	63	29	29
GR10	17	21	21	20	23	22	21	23	23	8	38
Flow, m/s	0.4	0.8	1.2	0.4	0.8	1.2	0.4	0.8	1.2	0.8	
Press, kPa	345	345	345	690	690	690	1,035	1,035	1,035	345	
Order	3	1	2	6	4	5	9	7	8	10	

least effective with high MWCO (>30,000) membranes which were fouled by pore plugging. Cleaning would have also required longer stabilization periods for each set of operating conditions increasing the potential of problems associated with aging feed samples.

The TMP range was limited to 345–1,035 kPa (50–150 psig) due to the operating limits of plate and frame or tubular modules. Spiral-wound modules would not be suitable for this feed due to the potential for channel plugging and need for extensive pretreatment to remove suspended solids. The upper limit of the cross-flow velocity was determined by the pressure drop in the test cells and pumping capacity. The lower limit of 0.4 m/s was chosen because concentration polarization becomes significant under these conditions even with very low (200 ppm) concentrations of polyethylene glycol in the test cells used.

5. Results and Discussion

5.1. Flux loss ratios

The flux loss ratios for the different fouling mechanisms are summarized in Table 2 and were evaluated at a fixed set of operating conditions, 345 kPa and 0.8 m/s. The relationship between membrane material and adsorptive fouling is illustrated by the D_a terms. Low adsorptive fouling was observed with regenerated cellulose membranes with D_a ranging from −13 to 11%. Regenerated cellulose membranes have often been shown to exhibit low adsorptive fouling, particularly with proteins [3,20]. Flux loss ratios for the GR40 and GR10 membranes were not determined. However, polysulfones exhibited severe adsorptive fouling with PSFP; J_a/J_0 ratios averaged 41% and 22% for polysulfone and polyethersulfone, respectively [21].

The effect of the pore size or MWCO on the flux loss ratios is largely seen in the D_{pp} term. High MWCO membranes such as the HFM180 have significant pore plugging, D_{pp}=81%. Membranes such as the PLAC have significant D_m and D_{cp} terms. The PLAC membrane material (regenerated cellulose) and MWCO (1,000 Daltons) suggest that both D_a and D_{pp} would be minimal.

The relative magnitudes of each fouling resistance would change under different operating conditions. The D_{cp} term would increase at lower

CFVs or higher TMPs. Higher pressures would also increase the D_{pp} term for open membranes such as the HFM180 or GR40.

A D_a term was not given for the Desal 5 and G50 membranes because of the unusual behavior where $J_a > J_0$. The experimental procedure where coupons are removed and re-installed may account for small changes in the flux. Cases with J_a/J_0 ratios >1.4 were attributed changes in the membrane morphology. The membranes were pressurized with RO water for 5 h but not cleaned prior to adsorption tests. This is an unlikely cause of $J_a > J_0$ as it is difficult to argue that PSFP had any cleansing ability. A detailed discussion on this behavior was given in a previous article [21].

5.2. Changes in flux

The flux data for the various combinations of operating conditions are summarized in Table 3. Patterns in flux behavior are more easily seen in graphical form, and several cases will be highlighted. The changes in membrane performance were highly dependent on the membrane and the flux loss ratios.

The flux is shown as a function of the CFV and TMP for the LSY PVD1 membrane in Fig. 6. At a cross-flow velocity of 1.2 and 0.8 m/s the flux shows a limiting behavior above 690 kPa. When the TMP was increased from 345 kPa to 690 kPa, the flux increased from ~27 LMH to 48 and 54 LMH at 0.8 and 1.2 m/s, respectively. At the lowest cross-flow velocity, the limiting flux had almost been attained at 345 kPa. A three-fold increase in the TMP only increased the flux from 24 to 34 LMH rather than the 75 LMH expected in the absence of polarization effects.

The behavior of the LSY PVD1 membrane was consistent with its flux loss ratios. At the standard conditions the flux was dominated by D_m and Da. At 345 kPa the cross-flow velocity had no effect on the flux as would be expected as D_{cp} = −1%. As the TMP was increased at 0.4 m/s, D_{cp} began to dominate as more material was transported to the membrane surface and the

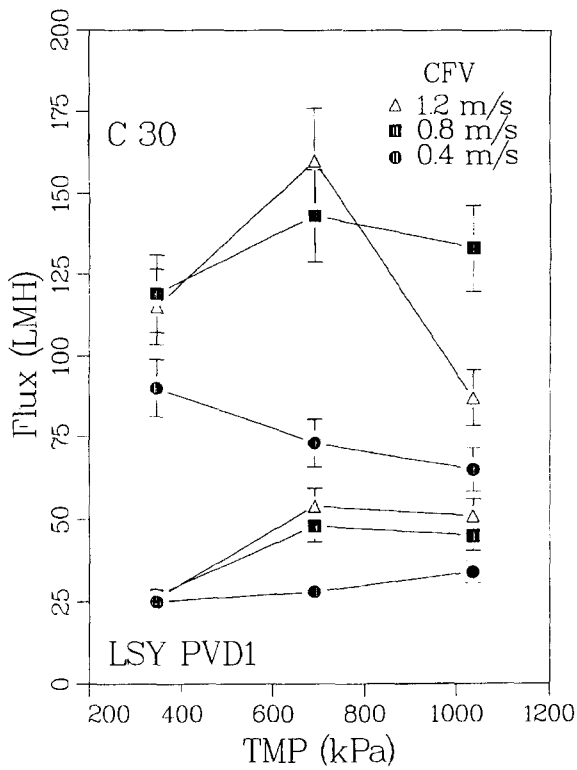

Fig. 6. Flux behavior of LSY PVD1 and C-30 at various operating conditions.

limiting flux was reached. Under these conditions increasing the CFV from 0.4 to 0.8 m/s did increase the flux.

The C-30 membrane exhibited unusual behavior; at 0.4 m/s the flux decreased slightly at higher pressures (Fig. 6). At 0.8 m/s the flux increased only slightly at higher TMPs. At 1.2 m/s the flux exhibited a noticeable maximum at 690 kPa dropping to less than the 0.8 m/s flux at 1,035 kPa. Similar behavior was observed with the C-10, G50 and PLAC membranes.

The flux behaviour of the GR10 membrane is shown in Fig. 7. The overall impression is that the flux is insensitive to the operating conditions. While the flux loss ratios for the GR10 membrane were not determined, one can predict that D_a and then D_{pp} would dominate given that the membrane material is polysulfone and the high 500,000

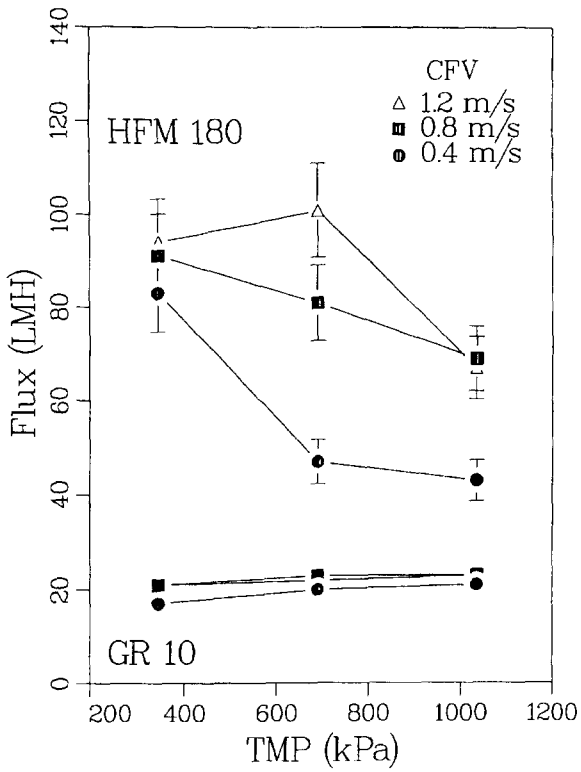

Fig. 7. Flux behavior of HFM 180 and GR10 at various operating conditions.

MWCO. The flux would not be expected to change significantly in this situation. Unlike the LSY PVD1 membrane, increasing the TMP with the GR10 membrane would only increase D_{pp}. Therefore, increasing the cross-flow velocity would not be expected to increase the flux.

The flux of the HFM180 membrane was dominated by pore plugging with D_{pp} = 81% (Fig. 7). The flux changed little at 345 kPa when the cross flow velocity was increased as D_{cp} was relatively small at 20%. At a given CFV, the flux decreased as the TMP was increased. This was not unexpected given that pore plugging was the dominant flux decline mechanism, even at the lowest TMP. The high MWCO also suggested that pore plugging would become more dominant at the higher pressures.

High MWCO membranes typically have wide pore size distributions, skewed toward the larger pores [11,22–25]. Pore plugging would reduce the effective pore size, predominantly blocking the largest pores. The larger pores, while representing a small fraction of the total number of pores, account for a much larger fraction of the total flow. Blocking the larger pores can greatly reduce the flux as was seen with the HFM180. This behavior was also observed for several other membranes, GR40, C-10, C-30 and PLAC membranes at higher TMPs. This behavior was expected for the GR40 because of its high MWCO rating of 100,000 but not for the PLAC and C-10 (1,000 and 10,000 MWCO, respectively). The pore plugging observed with lower MWCO membranes was most likely the result of the wide range of solute sizes in PSFP and did not become a problem until the highest TMP was used.

Pore plugging appears to have been a function of time as well as pressure. Pore plugging occurred rapidly at a given pressure with the HFM180 because of its high MWCO, but occurred at a slower rate with lower MWCO membranes and only at higher pressures. The unusual behavior of the C-30, C-10, G50 and PLAC membranes described earlier is most likely due to insufficient stabilization times, particularly at 1,035 kPa. The flux with these membranes at 1,035 kPa was not correlated with the CFV as would be expected. Instead the flux decreased as a function of the run order.

5.3. Changes in retention

Retentions based on TOC are reported in Table 4. The retention data are categorized by the TMP and further sorted according to the CFV at a given TMP. Given the ±5% accuracy of the retentions, a overall change of 10% is required before a significant change can be assumed at a given TMP. Cases where the CFV had a significant effect on retention are shaded. For example, the cross-flow velocity had an effect on the retention with the HFM180 membrane at 345 kPa but not at 690 or 1,035 kPa.

Table 4
TOC retentions of various membranes with PSFP at different operating conditions. Data are sorted based on the TMP and increasing cross-flow velocity at a given TMP and then by time on-line which corresponds to the run number.

Membrane	Retention (%)									
LSY PVD1	88	88	89	92	91	91	95	91	94	90
DESAL 5	92	91	92	94	94	93	97	93	96	96
PLAC	50	56	67	74	66	68	85	67	73	71
T66	77	75	80	85	81	83	88	85	88	85
C-10	34	35	43	57	45	44	61	52	55	54
G50	71	64	73	81	77	77	82	81	82	80
T64	80	77	79	86	82	82	90	86	88	88
C-30	30	25	39	52	36	40	66	52	50	51
HFM180	49	38	54	66	58	60	66	60	63	56
GR40	43	25	53	63	58	55	70	62	68	60
GR10	66	42	65	69	59	62	79	67	68	76
Flow, m/s	0.4	0.8	1.2	0.4	0.8	1.2	0.4	0.8	1.2	0.8
Press. kPa	345	345	345	690	690	690	1 035	1 035	1 035	345

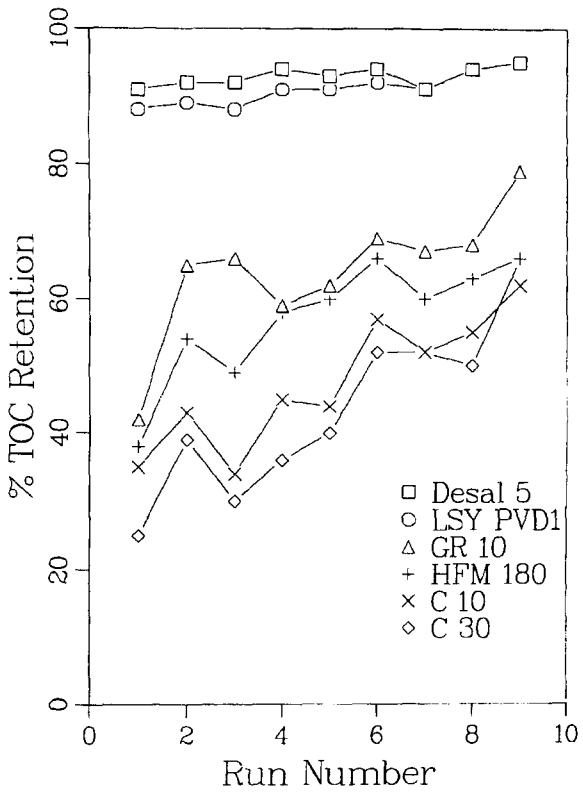

Fig. 8. TOC retention as a function of the run number.

The effect of cross-flow velocity and trans-membrane pressure on membrane flux have been shown to depend on the flux loss ratios for a given membrane.

Pore plugging was a significant fouling mechanism with a wide range of MWCOs and was attributed to the wide particle and solute size distribution of PSFP. High MWCO (>50,000 Da) membranes with significant D_{pp} terms were susceptible to pore plugging at 345 kPa. Membranes with MWCOs as low as 1,000 Da were affected by pore plugging but required higher TMPs. Insufficient time was allowed for pore plugging to stabilize at high TMPs for these membranes.

The resistance due to polarization began to control the flux at higher TMPs in the absence of pore plugging. When the "limiting flux" was reached, higher cross-flow velocities were required to attain higher fluxes. Fluxes showed little change or decreased in response to changing operating conditions with membranes for which D_a and D_{pp} dominated.

Retentions based on TOC reduction generally increased at higher TMPs. Retentions increased by ~ 20% to ~ 45% for open membranes with smaller increases (e.g., 6%) with tight membranes (<1,000 Da MWCO). This was the result of pore plugging changing the pore size distribution, particularly with high MWCO membranes. Retentions did not decrease with higher cross-flow velocities at a given pressure as would be expected in the case of concentration polarization or osmotic pressure limited flux. This suggests that that pore plugging may have been continuing and that a gel or cake layer was determining the retention. The presence of large particles, gel forming lignins and the RFA action as a binder further support the formation of a gel or cake.

Selection of an appropriate membrane for ultrafiltering PSFP requires attention to all aspects of the membrane and the operating conditions. RFAs and other organic compounds resulted in severe adsorptive fouling with several membrane materials. The solute size distribution also required that the membrane pore size or MWCO and TMP be considered simultaneously to avoid pore plugging. Module hydrodynamics (configuration and CFV) must also be optimized to minimize gel or cake formation.

High TOC retentions (96%) were obtained with the Desal 5 membrane with a flux of 82 LMH at 1,035 kPa, 1.2 m/s CFV and 50°C. Negligible flux decline was observed with this membrane, the material and MWCO (200 Da) minimized adsorption and pore plugging. However, this membrane could not be used in its typical spiral wound configuration without significant pretreatment. The highest flux was obtained with a C-30 membrane, 160 LMH at 690 kPa, 1.2 m/s CFV and 50°C, but the retention was much lower at 52%. Long-term testing must be undertaken to verify that pore plugging would not progress further with this membrane.

7. Symbols

C_b — solute concentration in the bulk solution, kg/m^3
C_m — solute concentration at the membrane surface, kg/m^3
C_p — solute concentration in the permeate, kg/m^3
D — solute diffusivity, kg/m^3
d_h — hydraulic diameter, m
d_p — particle diameter, m
f — intrinsic retention
F — observed retention
H — flow channel height at perimeter of test cell, m
J_a — PWP after adsorptive fouling, l/m^2/h
J_f — PWP of membrane after permeation with feed solution, l/m^2/h
J_v — Product rate, l/m^2/h; flux through a membrane with any type of feed solution
J_o — Pure water permeation rate, l/m^2/h; flux through a membrane with pure water only
k — mass transfer coefficient, m/s
k_B — Boltzman constant, J/K
LMH — flux, l/m^2/h
MWCO — molecular weight cut off, Daltons; by convention, the molecular weight at which a membrane retains 90% of that solute
ΔP — transmembrane pressure drop, driving force for permeation
r — internal radius of a hollow fiber, m
Re — Reynolds number
R_a — serial resistance due to adsorptive fouling, s^{-1}
R_h — serial resistance due to osmotic pressure or gel/cake layer, s^{-1}
R_m — hydraulic resistance of a new membrane, s^{-1}
R_{pp} — serial resistance due to pore plugging, s^{-1}
Sc — Schmidt number
Sh — Sherwood number
u_0 — bulk feed flow velocity, m/s

Greek

δ — thickness of the polarized layer, m
μ_b — viscosity of bulk feed solution, kg/m/s
μ_m — viscosity of feed solution at the membrane surface, kg/m/s
ρ — density, kg/m^3
υ_B — Brownian diffusion, solute/particle back transport velocity, m/s
υ_L — Lateral transport velocity of solute/particle, m/s
υ_S — shear induced solute/particle back transport velocity, m/s

Acknowledgements

The authors would like to acknowledge Hervé Buisson of the Wastewater Treatment Centre for membrane samples and helpful discussions. Also, from I.C.P.E.T., we would like to thank: Chung Ming Tam and Ashwani Kumar for discussions, Joanne Richard and Karen Lamb for performing permeation experiments and John Woods for GPC analysis.

References

[1] J.H. Hanemaaijer, T. Robbertsen, Th. van den Boomgaard and J.W. Gunnink, Desalination, 68 (1989) 199.
[2] C.M. Tam and A.Y. Tremblay, J. Membr. Sci., 57 (1991) 271.
[3] S. Nakatsuka and A. S. Michaels, J. Membr. Sci., 69 (1992) 189.
[4] G. Belfort, J.M. Pimbley, A. Greiner and K.Y. Chung, J. Membr. Sci., 77 (1993) 1.
[5] W.F. Blatt, A. Dravid, A.S. Michaels and L. Nelsen, in: J.E. Flinn (ed.), Membrane Science and Technology, Plenum Press, New York, 1970, p. 47.
[6] C.W. van Oers, M.A.G. Vorstman, W.G.H.M. Muijselaar and P.J.A.M. Kerkhof, J. Membr. Sci., 73 (1992) 231.
[7] A.R. Da Costa, A.G. Fane and D.E. Wiley, J. Membr. Sci., 76 (1993) 245.
[8] V.G.J. Rodgers and R.E. Sparks, AIChEJ., 37(10) (1991) 1517.
[9] E. Spiazzi, J. Lenoir and A. Grangeon, J. Membr. Sci., 80 (1993) 49.

[10] H.B. Winzeler and G. Belfort, J. Membr. Sci., 80 (1993) 35.
[11] A.G. Fane, C.J.D. Fell and A.G. Waters, J. Membr. Sci. 9 (1981) 245.
[12] A.-S. Jönsson, J. Membr. Sci. 79 (1993) 93.
[13] A.S. Michaels, Chem. Engng. Prog. 64(12) (1968) 31.
[14] V. Gekas and B. Hallström, J. Membr. Sci. 30 (1987) 153.
[15] P. Aimar and R. Field, Chem. Eng. Sci., 47(3) (1992) 579.
[16] V. Lahoussine-Turcaud, M.R. Wiesner and J-Y. Bottero, J. Membr. Sci., 52 (1990) 173.
[17] P. Ramamurthy, R. Poole and J.G. Dorica, J. Pulp Pap. Sci., 21(2) (1995) 50.
[18] D. Woerner and J.L. McCarthy, AIChE Symp. Ser. 232(80) (1984) 25.
[19] D. Woerner and J.L. McCarthy, Tappi J. 70(3) (1987) 126.
[20] M.K. Ko and J.J. Pellegrino, J. Membr. Sci., 74 (1992) 141.
[21] M.M. Dal-Cin, C.N. Striez, T.A. Tweddle, C.E. Capes, F. McLellan, and H. Buisson, Desalination, 101 (1995) 155.
[22] M. Meireles, P. Aimar and V. Sanchez, J. Membr. Sci., 56 (1991) 13.
[23] M. Meireles, P. Aimar and V. Sanchez, J. Membr. Sci., 91 (1994) 293.
[24] K.M. Persson, G. Capanelli, A. Bottino and G. Trägårdh, J. Membr. Sci., 76 (1993) 61.
[25] L.E.S. Brink, S.J.G. Elbers, T. Robbertsen and P. Both, J. Membr. Sci., 76 (1993) 281.